LETTERS

Anderson localization of a non-interacting Bose–Einstein condensate

Giacomo Roati[1,2], Chiara D'Errico[1,2], Leonardo Fallani[1,2], Marco Fattori[1,2,3], Chiara Fort[1,2], Matteo Zaccanti[1,2], Giovanni Modugno[1,2], Michele Modugno[1,4,5] & Massimo Inguscio[1,2]

Anderson localization of waves in disordered media was originally predicted[1] fifty years ago, in the context of transport of electrons in crystals[2]. The phenomenon is much more general[3] and has been observed in a variety of systems, including light waves[4,5]. However, Anderson localization has not been observed directly for matter waves. Owing to the high degree of control over most of the system parameters (in particular the interaction strength), ultracold atoms offer opportunities for the study of disorder-induced localization[6]. Here we use a non-interacting Bose–Einstein condensate to study Anderson localization. The experiment is performed with a one-dimensional quasi-periodic lattice—a system that features a crossover between extended and exponentially localized states, as in the case of purely random disorder in higher dimensions. Localization is clearly demonstrated through investigations of the transport properties and spatial and momentum distributions. We characterize the crossover, finding that the critical disorder strength scales with the tunnelling energy of the atoms in the lattice. This controllable system may be used to investigate the interplay of disorder and interaction (ref. 7 and references therein), and to explore exotic quantum phases[8,9].

The transition between extended and localized states originally studied by Anderson for non-interacting electrons has not been directly observed in crystals, owing to the high electron–electron and electron–phonon interactions[2]. Researchers have therefore turned their attention to systems where interactions or nonlinearities are almost absent. Evidence of the Anderson localization for light waves in disordered media has been provided by an observed modification of the classical diffusive regime, featuring a conductor–insulator transition[4,5]. However, a clear understanding of the interplay between disorder and nonlinearity is considered crucial in contemporary condensed matter physics. First effects of weak nonlinearities have been recently shown in experiments with light waves in photonic lattices[10,11]. The combination of ultracold atoms and optical potentials offers a novel platform for the study of disorder-related phenomena where most of the relevant physical parameters, including those governing interactions, can be controlled[6,8]. The introduction of laser speckles[12] and quasi-periodic optical lattices[9] has made possible the investigation of the physics of disorder. The investigations reported so far have explored either quantum phases induced by interaction[9] or regimes of weak interaction where the observation of Anderson localization was precluded either by the size of the disorder or by delocalizing effects of nonlinearity[12–16].

In this work, we use a Bose–Einstein condensate in which the interactions can be tuned independently of the other parameters[17], to study localization due purely to disorder. We study localization in a one-dimensional lattice perturbed by a second, weak incommensurate lattice, which constitutes an experimental realization of the non-interacting Harper[18] or Aubry–André model[19]. This quasi-periodic system displays a transition from extended to localized states analogous to the Anderson transition, already in one dimension[20,21], whereas in the case of pure random disorder, more than two dimensions would be needed[22]. We clearly observe this transition by studying transport and both spatial and momentum distributions, and we verify the scaling behaviour of the critical disorder strength. Our system is described by the Aubry–André hamiltonian

$$H = J\sum_m (|w_m\rangle\langle w_{m+1}| + |w_{m+1}\rangle\langle w_m|) + \Delta\sum_m \cos(2\pi\beta m + \phi)|w_m\rangle\langle w_m| \quad (1)$$

where $|w_m\rangle$ is the Wannier state localized at the lattice site m, J is the site-to-site tunnelling energy, Δ is the strength of the disorder, $\beta = k_2/k_1$ is the ratio of the two lattice wave numbers, and ϕ is an arbitrary phase. In the experiment, the two relevant energies J and Δ (see Fig. 1a) can be controlled independently by changing the heights of the primary and secondary lattice potentials, respectively. For a maximally incommensurate ratio $\beta = (\sqrt{5}-1)/2$, the model exhibits a sharp transition from extended to localized states at $\Delta/J = 2$ (refs 18, 19, 21). For the actual experimental parameters, $\beta = 1.1972\ldots$ and the transition is broadened and shifted towards larger values of Δ/J (see Fig. 1b). Owing to the quasi-periodic nature of the potential, these localized states appear approximately every five sites (2.6 μm).

The non-interacting Bose–Einstein condensate is prepared by sympathetically cooling a cloud of interacting ^{39}K atoms in an optical trap, and then tuning the *s*-wave scattering length almost to zero by means of a Feshbach resonance[17,23] (see Methods). The spatial size of the condensate can be controlled by changing the harmonic confinement provided by the trap. For most of the measurements the size along the direction of the lattice is $\sigma \approx 5\,\mu$m. The quasi-periodic potential is imposed by using two lasers in a standing-wave configuration[16]. The gaussian shape of the laser beams forming the primary lattice also provides radial confinement of the condensate in the absence of the harmonic trap.

In our first experiment we investigated transport, by abruptly switching off the main harmonic confinement and letting the atoms expand along the one-dimensional bichromatic lattice. We detect the spatial distribution of the atoms at increasing evolution times using absorption imaging (see Fig. 2a). In a regular lattice ($\Delta = 0$) the eigenstates of the potential are extended Bloch states, and the system expands ballistically. In the limit of large disorder ($\Delta/J > 7$) we observe no diffusion, because in this regime the condensate can be described as the superposition of several localized eigenstates whose individual extensions are less than the initial size of the condensate. In the crossover between these two regimes we observe a ballistic expansion with reduced speed. This crossover is summarized in Fig. 2b, which, for a fixed evolution time of 750 ms, shows the width of the atomic distribution versus the rescaled disorder strength Δ/J,

[1]LENS and Dipartimento di Fisica, Università di Firenze, 50019 Sesto Fiorentino, Italy. [2]INFM-CNR, 50019 Sesto Fiorentino, Italy. [3]Museo Storico della Fisica e Centro Studi e Ricerche 'E. Fermi', 00184 Roma, Italy. [4]Dipartimento di Matematica Applicata, Università di Firenze, 50139 Firenze, Italy. [5]BEC-INFM Center, Università di Trento, 38050 Povo, Italy.

for three different values of J. In all three cases, the system enters the localized regime at the same disorder strength, providing compelling evidence of the scaling behaviour intrinsic to the model described in equation (1).

In this regime, the eigenstates of the hamiltonian in equation (1) are exponentially localized, and the tails of diffusing wave packets are expected to behave like stretched exponentials[24]. We therefore analysed the tails of the spatial distributions with an exponential function of the form $f_\alpha(x) = A\exp(-|(x-x_0)/l|^\alpha)$, the exponent α being a fitting parameter. Two examples of this analysis, one for weak disorder and one for strong disorder, are shown in Fig. 3a, b. The exponent α exhibits a smooth crossover from a value of two to a value of one as Δ/J increases (Fig. 3c), signalling the onset of an exponential localization. The value $\alpha = 2$ that we obtain for small Δ/J corresponds to the expected ballistic evolution of the initial gaussian momentum distribution of the non-interacting condensate. We note that in the radial direction, where the system is only harmonically trapped, the spatial distribution is always well fitted by a gaussian function ($\alpha = 2$).

Information on the eigenstates of the system can also be extracted from the analysis of the momentum distribution of the stationary atomic states in the presence of the harmonic confinement. The width of the axial momentum distribution $P(k)$ is inversely proportional to the spatial extent of the condensate in the lattice. We measure it by releasing the atoms from the lattice and imaging them after a ballistic expansion.

In Fig. 4, we show examples of the experimental momentum distributions that are in agreement with the model predictions for the low-lying eigenstates. Without disorder, we observe the typical grating interference pattern with three peaks at $k = 0, \pm 2k_1$, reflecting the periodicity of the primary lattice. The very small width of the peak at $k = 0$ indicates that the wavefunction is spread over many lattice sites[25]. For weak disorder, the eigenstates of the hamiltonian in equation (1) are still extended, and additional momentum peaks appear at momentum space distances $\pm 2(k_1 - k_2)$ from the main peaks, corresponding to the beating of the two lattices. As we further increase Δ/J, $P(k)$ broadens and its width eventually becomes comparable with that of the Brillouin zone, k_1, indicating that the extension of the localized states becomes comparable with the lattice spacing. From the theoretical analysis of the Aubry–André model, we have a clear indication that in this regime the eigenstates are exponentially localized on individual lattice sites.

We note that the side peaks in the two bottom profiles of Fig. 4a, b indicate that the localization is non-trivial, that is, the tails of the eigenstates extend over several lattice sites even for large disorder. The small modulation on top of the profiles is due to the interference between the several localized states over which the condensate is distributed. In Fig. 4c, we present the root-mean-squared width of the central peak of $P(k)$ as a function of Δ/J, for three different values of J. The three data sets lie on the same line, confirming the scaling behaviour of the system. A visibility of the interference pattern,

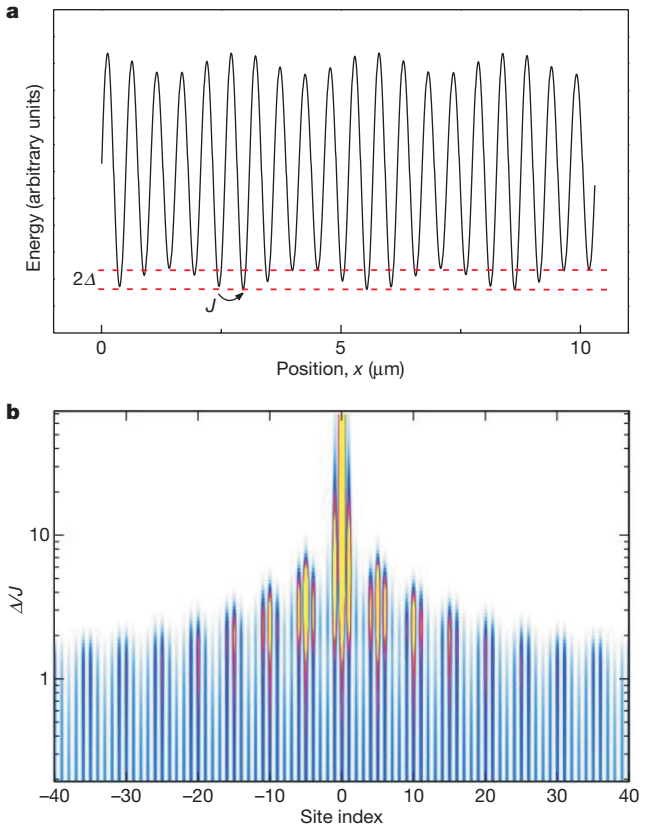

Figure 1 | The quasi-periodic optical lattice. a, The quasi-periodic potential realized in the experiment. The hopping energy J describes the tunnelling between different sites of the primary lattice and 2Δ is the maximum shift of the on-site energy induced by the secondary lattice. The lattice constant is 516 nm. **b**, Typical calculated density plot of a low-lying eigenstate of the bichromatic potential, as a function of Δ/J (vertical axis). For small values of Δ/J the state is delocalized over many lattice sites. For $\Delta/J \geq 7$ the state becomes exponentially localized on lengths smaller than the lattice constant.

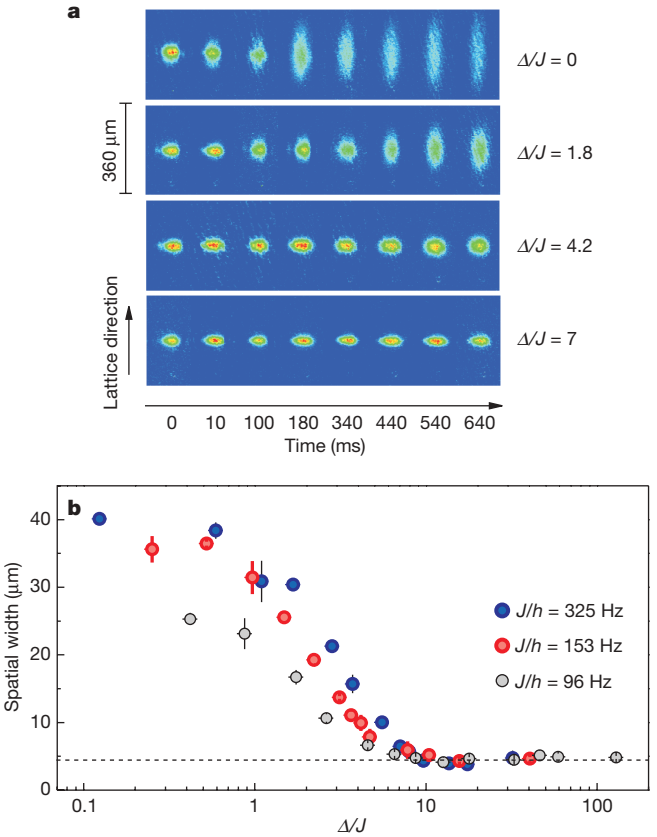

Figure 2 | Probing the localization with transport. a, *In situ* absorption images of the Bose–Einstein condensate diffusing along the quasi-periodic lattice for different values of Δ and $J/h = 153$ Hz (where h denotes Planck's constant). For $\Delta/J > 7$ the size of the condensate remains at its original value, reflecting the onset of localization. **b**, Root-mean-squared size of the condensate for three different values of J, at a fixed evolution time of 750 ms, versus the rescaled disorder strength Δ/J. The dashed line indicates the initial size of the condensate. The onset of localization appears in the same range of values of Δ/J in all three cases. Vertical error bars, 95% confidence level (± 2 s.e.m.); horizontal error bars, 10% uncertainty due to the nonlinearity of the modulators' response.

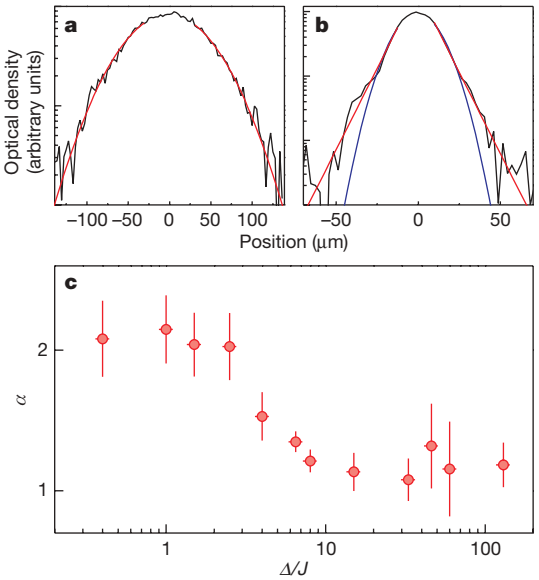

Figure 3 | Observing the nature of the localized states. **a**, **b**, Experimental profiles and fitting function $f_\alpha(x)$ (red) for $\Delta/J \approx 1$ (**a**) and $\Delta/J \approx 15$ (**b**). Note the vertical log scale. The blue line in **b** represents a gaussian fit, $\alpha = 2$. **c**, Dependence of the fitting parameter α on Δ/J, indicating a transition from a gaussian to an exponential distribution. Vertical error bars, 95% confidence level (± 2 s.e.m.); horizontal error bars, 10% uncertainty due to the nonlinearity of the modulators' response.

$V = (P(2k_1) - P(k_1))/(P(2k_1) + P(k_1))$, can be defined to highlight the appearance of a finite population in the momentum states $\pm k_1$ and, therefore, the onset of exponential localization with an extension comparable with the lattice spacing. In Fig. 4d, we show the visibility extracted from the same data as Fig. 4c. Experiment and theory are again in good agreement, and feature a sudden decrease in the visibility for $\Delta/J \approx 6$.

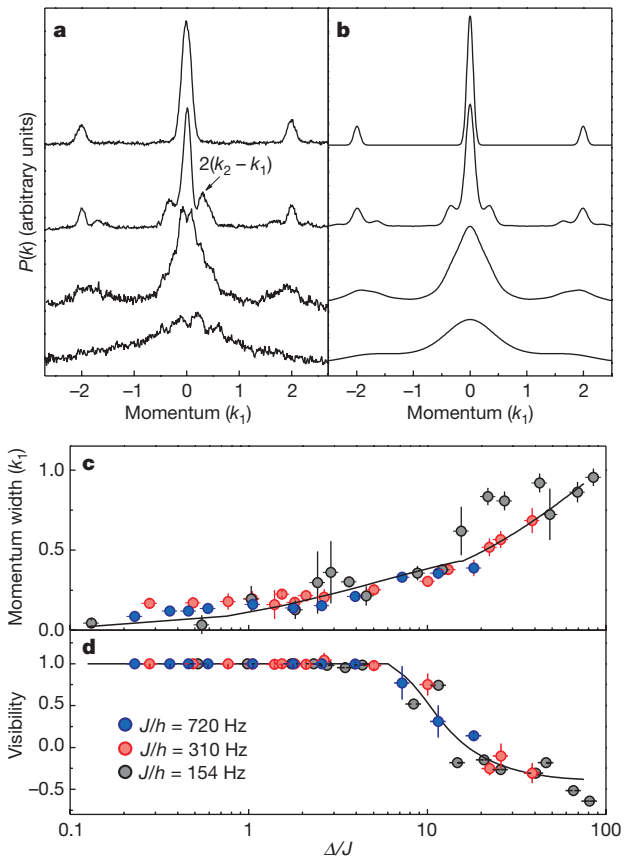

Figure 4 | Momentum distribution. **a**, **b**, Experimental and theoretical momentum distributions $P(k)$ for increasing Δ/J values (0, 1.1, 7.2 and 25, from top to bottom). The interference pattern of a regular lattice observed at $\Delta = 0$ is at first modified by the appearance of peaks at the beating between the two lattices, and then increasingly broadened. Momentum is measured along the horizontal axes in units of k_1. **c**, Root-mean-squared size of the central peak of $P(k)$ versus Δ/J, for three different values of J. The experimental data follow a unique scaling behaviour, as predicted by theory (continuous line). The width of the peak is measured in units of k_1. **d**, Visibility V of the interference pattern versus Δ/J. In both experiment and theory (continuous line), V decreases abruptly for $\Delta/J \approx 6$, indicating localization on distances comparable to the lattice period. Vertical error bars, 95% confidence level (± 2 s.e.m.); horizontal error bars, 10% uncertainty due to the nonlinearity of the modulators' response.

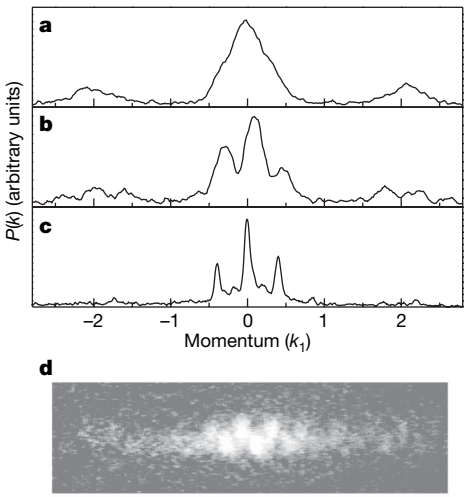

Figure 5 | Interference of localized states. Momentum distribution of the condensate prepared in a disordered lattice with $\Delta/J \approx 10$, for different values of the harmonic confinement. **a**, Profile of a single localized state (initial spatial size of the condensate, $\sigma = 1.2$ μm); **b**, interference of two localized states ($\sigma = 1.2$ μm); **c**, interference of three localized states ($\sigma = 2.1$ μm). Momentum is measured along the horizontal axes in units of k_1. **d**, Dislocated interference pattern resulting from the interference of two localized states, suggesting the presence of a thermally activated vortex.

Further information on the localized states can be extracted from the interference of a small number of them. This regime can be reached in the experiment by simply reducing the spatial extent of the condensate through an increase of the harmonic confinement. Typical profiles of $P(k)$ are displayed in Fig. 5a–c. Depending on the degree of confinement, we observe one, two or three states, featuring a smooth distribution or a clear multiple-slit interference pattern. The spacing of the fringes yields a spatial separation between the localized states of about five sites, as expected. The independent localized states have a quasi-two-dimensional geometry, because their axial extents are much smaller than their radial extents. This feature makes our system an excellent testing ground in which to study the physics of quasi-two-dimensional systems[26], which were recently investigated using widely spaced optical lattices[27]. We also observe (Fig. 5d) interference patterns which present a dislocation, possibly produced by thermal activation of a vortex in one of the two localized states[27], but in our case for non-interacting atoms.

In this work we have observed Anderson localization of coherent non-interacting matter waves. Future studies might reveal how a weak, controllable interaction affects the observed localization transition. More generally, the high theoretical and experimental control possible in this system makes it a novel platform for the study of exotic quantum phases arising from the interplay between interaction and disorder[6,8,28] (see also ref. 29 and references therein).

METHODS SUMMARY

Non-interacting Bose–Einstein condensate. The condensate of ^{39}K atoms was produced at a large positive value of the *s*-wave scattering length ($a \approx 180a_0$, $a_0 = 0.529 \times 10^{-10}$ m) at a magnetically tuneable Feshbach resonance[17,30]. The scattering length was then adiabatically reduced to values of the order of $0.1a_0$ (ref. 23), corresponding to an atom–atom interaction energy of $U \approx 10^{-5}J$ (ref. 6).

Quasi-periodic optical lattice. The quasi-periodic potential was created by superimposing two standing waves created with laser beams of wavelengths $\lambda_1 \approx 1{,}032$ nm (primary lattice) and $\lambda_2 \approx 862$ nm (secondary lattice), with waists of 150 μm. The two lattice depths were adjusted by varying the intensity of the beams, and calibrated by Bragg diffraction. The heights s_i of the lattices ($i = 1, 2$), in units of the recoil energies $E_{R,i} = h^2/(2M\lambda_i^2)$, are $s_1 \leq 10$ and $s_2 \leq 3$ (where M is the atomic mass). The estimated relative uncertainty at a 95% confidence level on Δ/J is 15%. An additional uncertainty of 10% due to the nonlinearity of the modulators' response is shown in Figs 2–4 as a horizontal error bar.

Analysing the atomic distributions. The atomic samples were imaged on a charge-coupled-device camera with a spatial resolution of about 5 μm. The images analysed in Figs 2 and 3 were recorded just after the release from the trap. The analysis of the profiles of Fig. 3 was carried out by integrating the atomic density distributions along the radial direction. The top 20% of the signal was dropped and only the remaining tails were fitted. This takes into account the possible gaussian broadening effects of the transfer function of the imaging system and the fact that we populate few localized states. The profiles in Figs 4 and 5 were obtained after a long ballistic expansion over 25 ms to reduce the contribution of the initial spatial distribution. The analysis of typically four or five different images was used to extract individual data points in Figs 2–4. The vertical error bars in Figs 2–4 correspond to a 95% confidence level (± 2 s.e.m.).

Full Methods and any associated references are available in the online version of the paper at www.nature.com/nature.

Received 31 March; accepted 6 May 2008.

1. Anderson, P. W. Absence of diffusion in certain random lattices. *Phys. Rev.* **109,** 1492–1505 (1958).
2. Lee, P. A. & Ramakrishnan, T. V. Disordered electronic systems. *Rev. Mod. Phys.* **57,** 287–337 (1985).
3. Kramer, B. & MacKinnon, A. Localization: theory and experiment. *Rep. Prog. Phys.* **56,** 1469–1564 (1993).
4. Van Albada, M. P. & Lagendijk, A. Observation of weak localization of light in a random medium. *Phys. Rev. Lett.* **55,** 2692–2695 (1985).
5. Wiersma, D. S., Bartolini, P., Lagendijk, A. & Righini, R. Localization of light in a disordered medium. *Nature* **390,** 671–673 (1997).
6. Damski, B., Zakrzewski, J., Santos, L., Zoller, P. & Lewenstein, M. Atomic Bose and Anderson glasses in optical lattices. *Phys. Rev. Lett.* **91,** 080403 (2003).
7. Dubi, Y., Meir, Y. & Avishai, Y. Nature of the superconductor-insulator transition in disordered superconductor. *Nature* **449,** 876–880 (2007).
8. Lewenstein, M. *et al.* Ultracold atomic gases in optical lattices: mimicking condensed matter physics and beyond. *Adv. Phys.* **56,** 243–379 (2007).
9. Fallani, L., Lye, J. E., Guarrera, V., Fort, C. & Inguscio, M. Ultracold atoms in a disordered crystal of light: towards a Bose glass. *Phys. Rev. Lett.* **98,** 130404 (2007).
10. Schwartz, T., Bartal, G., Fishman, S. & Segev, M. Transport and Anderson localization in disordered two-dimensional photonic lattices. *Nature* **446,** 52–55 (2007).
11. Lahini, Y. *et al.* Anderson localization and nonlinearity in one-dimensional disordered photonic lattices. *Phys. Rev. Lett.* **100,** 013906 (2008).
12. Lye, J. E. *et al.* Bose-Einstein condensate in a random potential. *Phys. Rev. Lett.* **95,** 070401 (2005).
13. Clément, D. *et al.* Suppression of transport of an interacting elongated Bose-Einstein condensate in a random potential. *Phys. Rev. Lett.* **95,** 170409 (2005).
14. Fort, C. *et al.* Effect of optical disorder and single defects on the expansion of a Bose-Einstein condensate in a one-dimensional waveguide. *Phys. Rev. Lett.* **95,** 170410 (2005).
15. Schulte, T. *et al.* Routes towards Anderson-like localization of Bose-Einstein condensates in disordered optical lattices. *Phys. Rev. Lett.* **95,** 170411 (2005).
16. Lye, J. E. *et al.* Effect of interactions on the localization of a Bose-Einstein condensate in a quasi-periodic lattice. *Phys. Rev. A* **75,** 061603 (2007).
17. Roati, G. *et al.* ^{39}K Bose-Einstein condensate with tunable interactions. *Phys. Rev. Lett.* **99,** 010403 (2007).
18. Harper, P. G. Single band motion of conduction electrons in a uniform magnetic field. *Proc. Phys. Soc. A* **68,** 874–878 (1955).
19. Aubry, S. & André, G. Analyticity breaking and Anderson localization in incommensurate lattices. *Ann. Israel Phys. Soc.* **3,** 133–140 (1980).
20. Grempel, D. R., Fishman, S. & Prange, R. E. Localization in an incommensurate potential: an exactly solvable model. *Phys. Rev. Lett.* **49,** 833–836 (1982).
21. Aulbach, C., Wobst, A., Ingold, G.-L., Hänggi, P. & Varga, I. Phase-space visualization of a metal–insulator transition. *New J. Phys.* **6,** doi:10.1088/1367-2630/6/1/070 (2004).
22. Abrahams, E., Anderson, P. W., Licciardello, D. C. & Ramakrishnan, T. V. Scaling theory of localization: absence of quantum diffusion in two dimensions. *Phys. Rev. Lett.* **42,** 673–676 (1979).
23. Fattori, M. *et al.* Atom interferometry with a weakly interacting Bose-Einstein condensate. *Phys. Rev. Lett.* **100,** 080405 (2008).
24. Zhong, J. *et al.* Shape of the quantum front. *Phys. Rev. Lett.* **86,** 2485–2489 (2001).
25. Pedri, P. *et al.* Expansion of a coherent array of Bose-Einstein condensates. *Phys. Rev. Lett.* **87,** 220401 (2001).
26. Burger, S. *et al.* Quasi-2D Bose-Einstein condensation in an optical lattice. *Europhys. Lett.* **57,** 1–6 (2002).
27. Hadzibabic, Z., Krüger, P., Cheneau, M., Battelier, B. & Dalibard, J. Berezinskii-Kosterlitz-Thouless crossover in a trapped atomic gas. *Nature* **441,** 1118–1121 (2006).
28. Lugan, P. *et al.* Ultracold Bose gases in 1D disorder: from Lifshits glass to Bose-Einstein condensate. *Phys. Rev. Lett.* **98,** 170403 (2007).
29. Roux, G. *et al.* The quasi-periodic Bose-Hubbard model and localization in 1-dimensional cold atomic gases. Preprint at ⟨http://arxiv.org/abs/0802.3774⟩ (2008).
30. D'Errico, C. *et al.* Feshbach resonances in ultracold ^{39}K. *New J. Phys.* **9,** doi:10.1088/1367-2630/9/7/223 (2007).

Acknowledgements We thank J. Dalibard for discussions, S. Machluf for contributions, and all the colleagues of the Quantum Gases group at LENS. This work has been supported by MIUR, EU (IP SCALA), ESF (DQS–EuroQUAM), INFN and Ente CRF.

Author Information Reprints and permissions information is available at www.nature.com/reprints. Correspondence and requests for materials should be addressed to M.I. (inguscio@lens.unifi.it).

METHODS

Non-interacting Bose–Einstein condensate. The condensate was prepared in a homogeneous magnetic field of about 396 G, where a broad Feshbach resonance raised the value of the *s*-wave scattering length from the background value of $-29a_0$ to about $180a_0$ (refs 17, 30). This allowed the efficient formation of a stable condensate. The condensate was trapped in a crossed dipole trap with an average harmonic frequency of 100 Hz, and contained about 10^5 atoms. The scattering length was then reduced by shifting the magnetic field to about 350 G, at the zero-crossing position. This magnetic field was adiabatically changed with a combined linear and exponential ramp lasting 110 ms, to avoid shape excitations of the cloud. We estimate a residual scattering length of the order of $0.1a_0$, limited by magnetic field instability (100 mG) and by the contribution to the scattering of higher-order partial waves.

Quasi-periodic lattice. The quasi-periodic lattice was created by superimposing two standing waves of incommensurate wavelengths. In particular, the primary lattice was generated by a single-mode Yb:YAG laser of wavelength $\lambda_1 = 1{,}032$ nm, whose linewidth and intensity were actively stabilized, and the secondary lattice was obtained by a single-mode Ti:Sapphire laser of wavelength $\lambda_2 = 862$ nm. The lattice beams were focused on the condensate with a beam waist of about 150 μm. In the absence of the harmonic trap, in the radial plane, the atoms felt a harmonic confinement of about 40 Hz due to the gaussian intensity profile of the laser beams of the primary lattice. The optical power in each of the two standing waves was independently adjusted by means of two acousto-optic modulators, and the lattice heights were calibrated by means of Bragg diffraction[31]. In the experiment, the primary lattice depth ranged up to 10 $E_{R,1}$, and that of the secondary lattice to 3 $E_{R,2}$, where $E_{R,i} = h^2/(2M\lambda_i^2)$ are the recoil energies ($i = 1, 2$). Before loading the condensate into the quasi-periodic lattice, we adiabatically reduced the harmonic trap frequency to 5 Hz by decreasing the intensity of the dipole trap beams. The lattices were then raised by means of 's'-shaped ramps, on a timescale of 100 ms.

Theory. Since our three-dimensional condensate is non-interacting, the problem is separable. Along the direction of the bichromatic lattice, the system is described by the single-particle hamiltonian $H_{1D} = -(h^2/(8\pi^2 M))\partial^2/\partial x^2 + s_1 E_{R,1}\cos^2(k_1 x) + s_2 E_{R,2}\cos^2(k_2 x)$, where $k_i = 2\pi/\lambda_i$ ($i = 1, 2$) are the lattice wavenumbers and s_i are the heights of the two lattices in units of the recoil energies $E_{R,i}$. In the tight-binding limit, the above hamiltonian can be mapped to the Aubry–André hamiltonian in equation (1), with $\Delta = s_2 E_{R,2}/(2E_{R,1})$ and $J \approx 1.43 {s_1}^{0.98} \exp(-2.07\sqrt{s_1})$ (ref. 32). Fig. 1b represents a typical density plot of a lowest lying eigenstate of the bichromatic potential, obtained by direct diagonalization of the full hamiltonian H_{1D}. The plots in Fig. 4b also include the effect of the harmonic trapping potential $V_{ho}(x) = M\omega^2 x^2/2$, with $\omega = 2\pi \times 5$ Hz.

Data analysis. The root-mean-squared widths presented in Fig. 2b were obtained by integrating the two-dimensional distributions of Fig. 2a in the radial direction, and by fitting the axial distribution with gaussian profiles. The analysis shown in Fig. 3 consisted of fitting only the tails of the axial distributions with an exponential decay of the form $f_z(x) = A\exp(-|(x - x_0)/l|^\alpha)$, leaving the exponent α as a fitting parameter. We exclude from the fit the central part of the distributions, within 0.6 times the root-mean-squared width from the centre. For our data, this choice represents the best compromise between dropping an expected gaussian component at the centre and having a sufficiently large dynamical range to fit the tails. The analysis of the data in Fig. 3 was based on the average of 4–5 different experimental images. All experimental momentum distribution profiles in Figs 4 and 5 were obtained by radial integration of the two-dimensional distributions. For the analysis in Fig. 4c, we directly measured the root-mean-squared width of the central peak when this could be resolved from the side peaks, or we fitted the overall distribution with three gaussian profiles to extract the width of the central peak. This procedure was applied to both experiment and theory.

31. Ovchinnikov, YuB *et al.* Diffraction of a released Bose-Einstein condensate by a pulsed standing light wave. *Phys. Rev. Lett.* **83**, 284–287 (1999).
32. Gerbier, F. *et al.* Interference pattern and visibility of a Mott insulator. *Phys. Rev. A* **72**, 053606 (2005).